Available online at www.sciencedirect.com
ScienceDirect
Trans. Nonferrous Met. Soc. China 33(2023) 2054−2063
Transactions of Nonferrous Metals Society of China
www.tnmsc.cn

Interfacial reaction in Al_2O_3 fiber reinforced TiAl matrix composite

Yao-feng LUO, Rui-yu LU, Yan WANG, Bin LIU, Hai-tang YANG, Yong LIU

State Key Laboratory of Powder Metallurgy, Central South University, Changsha 410083, China

Received 3 March 2022; accepted 15 July 2022

Abstract: Al_2O_3 short fiber (containing 28 vol.% SiO_2) reinforced TiAl matrix composite was prepared by spark plasma sintering (SPS). The interfacial reaction mechanism was clarified by thermodynamic and kinetic analyses. The main interfacial phase was Ti_5Si_3, originated from Ti element of TiAl matrix and Si element of Al_2O_3 fiber. The activation energy of interfacial layer was 285.1 kJ/mol. In addition, the matrix around the interfacial region was composed of γ-TiAl phase due to the consumption of Ti element in the process of interfacial reaction. However, the formation of mullite phase occurred in the heat-treated Al_2O_3 fiber and as-sintered composite due to the chemical reaction between γ-Al_2O_3 and amorphous SiO_2 phases.

Key words: TiAl-based composite; interfacial reaction mechanism; Al_2O_3 fiber; phase transformation; densification mechanism

1 Introduction

TiAl intermetallics are considered to be promising high temperature structural materials with the advantage of low density, high specific strength and stiffness, good oxidation resistance and creep resistance [1,2]. However, the high brittleness and poor forming ability hinder their practical applications [3,4]. Moreover, the fracture toughness of TiAl intermetallics must be further improved. Accordingly, many studies have addressed these problems on alloying [5,6] and adjusting the microstructures of TiAl intermetallics [7,8]. However, the toughening effect is limited. As a result, TiAl matrix composites, which can effectively improve the fracture toughness, are drawing more and more attention.

The reinforcements of TiAl matrix composites include particles [9], whiskers [10], and fibers [11]. YUAN et al [9] investigated the hot deformation behavior of Ta-particle reinforced Ti−48Al−2Cr−2Nb−0.2W composite, and found that the addition of plastic Ta particles was beneficial to the hot working of TiAl intermetallics. On the other hand, the fiber reinforced TiAl matrix composites can be toughened by bridging, crack bending and deflection, fiber debonding and pull-out [11]. The fiber reinforcement can be categorized into continuous (long) fiber reinforcement and discontinuous (short) fiber reinforcement. The continuous fiber reinforced composites have some problems, such as high cost, complex preparation process, difficulty in secondary processing and anisotropy of mechanical properties. However, discontinuous fiber reinforced composites can be more flexibly and simply processed. In addition, the mismatch sensitivity of thermal expansion coefficient between TiAl matrix and short fiber is low.

At present, some fiber reinforcements have been introduced to TiAl matrix composites, such as C, SiC, Mo, Ta, TiNb and Al_2O_3 fibers. C [12] and SiC [13] fibers have the advantages of low density and good thermal stability. However, the interfacial reaction between TiAl matrix and reinforcements is very severe, and the compatibility of the thermal

Corresponding author: Yong LIU, Tel: +86-731-88836939, E-mail: yonliu@csu.edu.cn
DOI: 10.1016/S1003-6326(23)66243-0

expansion coefficients is also a problem. Mo [14], Ta [11] and TiNb [15] fibers have high toughness, but large density. Among these reinforcements, Al_2O_3 fiber matches well with TiAl matrix in thermal expansion coefficient and elastic modulus, which can significantly reduce the thermal residual stress and formation of cracks at the interfacial region [16,17]. In addition, Al_2O_3 fiber possesses low density, high melting point and excellent mechanical properties [18]. CUI et al [10] investigated the effect of Al_2O_3 whiskers on mechanical properties of $Al_2O_{3,w}$/Ti−46Al−4Nb composites, and found that the introduction of Al_2O_3 whiskers can significantly enhance the comprehensive mechanical properties by fine-grain strengthening and whisker toughening. WEBER et al [16] demonstrated that continuous Al_2O_3 ceramic fibers can improve the creep property and fracture resistance of TiAl matrix by weak fiber−matrix interface. However, the interfacial reaction mechanism of Al_2O_3 with TiAl matrix has been rarely reported. Moreover, it is of significance to disclose the phase transformation of $Al_2O_{3,f}$/TiAl composite after interfacial reaction.

In this work, Al_2O_3 short fiber (containing 28 vol.% SiO_2) was introduced into TiAl matrix by spark plasma sintering (SPS). The SiO_2 phase in Al_2O_3 fibers was to inhibit the grain growth in the fabrication process, which made interfacial reaction more complicated. The microstructures of the interfacial reaction between TiAl matrix and Al_2O_3 fiber were investigated. Moreover, the interfacial reaction mechanism was also revealed by thermodynamic calculation and kinetic analyses. In addition, the phase transformation around the $Al_2O_{3,f}$/TiAl interface was also identified.

2 Experimental

2.1 Material preparation

Pre-alloyed TiAl powder with a nominal composition of Ti−45Al−7Nb−0.4W−0.1B (at.%) was fabricated by plasma rotating electrode process (PREP) technology. Figures 1(a−c) show that the average size of TiAl powder is 94 μm. It can be seen that TiAl powder is composed of γ and α_2 phases (Fig. 1(d)). Al_2O_3 fiber was produced by sol−gel method and electrospinning technology in Shanghai Rongrong Co. Ltd., China. Figure 1(e) shows the morphology of Al_2O_3 fiber. The diameter is about 16 μm, and the phases include γ-Al_2O_3 and amorphous SiO_2 (Fig. 1(f)).

The 1 vol.% Al_2O_3 short fibers (0.5−1 mm in length) and 99 vol.% TiAl powder were mixed at 30 r/min for 24 h in a mixer. Subsequently, 30 g mixtures were put into a graphite mold and sintered in an SPS apparatus (LABOX TM 325R, Japan) at a pressure of 40 MPa. The sintering temperatures were from 1050 to 1300 °C. The heating process included two stages: from room temperature to 600 °C at 50 °C/min, and from 600 °C to target sintering temperature at 80 °C/min. At sintering temperatures, the samples were held for 10 min. Finally, the samples were cooled down to room temperature in furnace. The $Al_2O_{3,f}$/TiAl composite with a diameter of 30 mm and a thickness of 10 mm was obtained. The relative density of composite was measured.

The high temperature thermal exposure experiments were performed for the composite sintered at 1100 and 1150 °C in order to study the interfacial reaction kinetics. The exposure time was from 0.5 to 3 h. It is worth noting that the Al_2O_3 fibers were also heat-treated at temperatures from 1050 to 1300 °C for 4 h in order to study the phase transition.

2.2 Microstructural characterization and hardness measurement

The microstructures of TiAl composite were characterized by using scanning electron microscopy (SEM, FEI Helios) and electron backscatter diffraction (EBSD, Oxford). For the EBSD characterization, polished specimens were etched by A3 reagent (90 vol.% ethanol and 10 vol.% perchlorate), and then electrolytically polished at 20 V for 20 s. The EBSD measurement was carried out at an accelerating voltage of 20 kV and with a step interval of 0.5 μm. Data from EBSD were further analyzed by using HKL Channel 5 software. The chemical compositions of composite were detected by electro-probe microanalyses (EPMA, JEOL). The phase constitutions of TiAl powder, Al_2O_3 fiber and composites were identified by using an X-ray diffractometer (XRD, Rigaku D/max 2550VB) with Cu K_α radiation. The scanning angle ranged from 10° to 90° with a scanning step interval of 0.02°. Jade 5.0 software was used to analyze the phase structures. The macro-hardness of composite was measured by Vickers hardness tester.

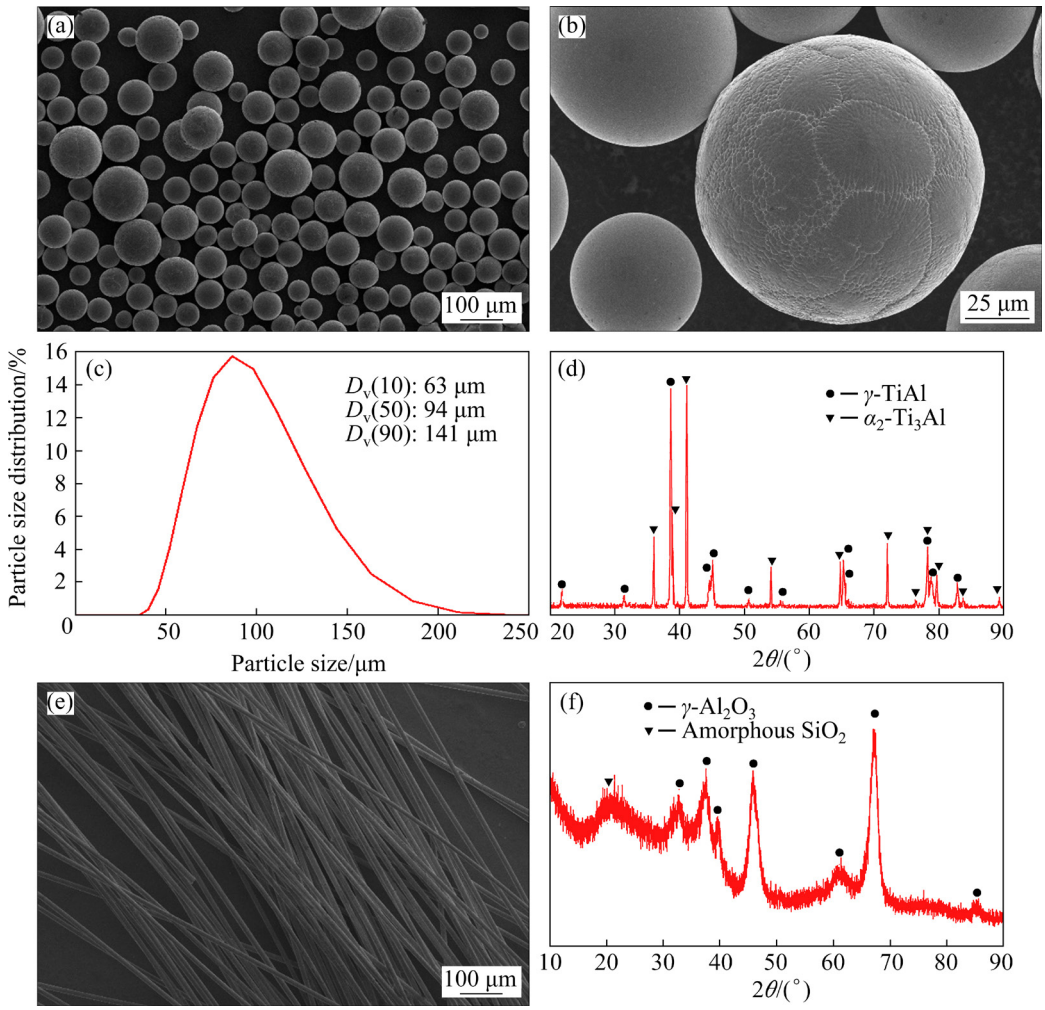

Fig. 1 Morphologies and phase compositions of Ti−45Al−7Nb−0.4W−0.1B pre-alloyed powder and Al_2O_3 fiber: (a) Morphology of TiAl powder at low magnification; (b) Morphology of TiAl powder at high magnification; (c) Size distribution curve of TiAl powder; (d) XRD patterns of TiAl powder; (e) Morphology of Al_2O_3 fiber; (f) XRD patterns of Al_2O_3 fiber

3 Results

3.1 Microstructures

Figure 2 shows the microstructures of as-sintered $Al_2O_{3,f}$/TiAl composite. At sintering temperature of 1050 °C, some obvious pores distribute in the composites, as indicated in Figs. 2(c, f). In the meantime, there exist some boundaries of primary TiAl particles in the matrix. At 1150 °C, the densification process is almost completed, and the composite exhibits a uniform γ phase microstructure. The interfacial reaction region is observed between Al_2O_3 fiber and TiAl matrix (Fig. 2(h)). With the increase of sintering temperature, the interfacial reaction becomes more and more severe, as shown in Figs. 2(j−l). The matrix microstructures of the composite sintered at 1300 °C transform from the near γ phase to fully lamellar structure (Fig. 2(l)).

Figure 3(a) displays the relative density of $Al_2O_{3,f}$/TiAl composite at various sintering temperatures. The density increases rapidly with the increase of temperature from 1050 to 1100 °C, then increases slowly from 1100 to 1200 °C, and finally remains constant in the range of 1200−1300 °C. The XRD patterns of as-sintered $Al_2O_{3,f}$/TiAl composite are shown in Fig. 3(b). Compared with that of TiAl powder in Fig. 1(d), the content of α_2 phase in the as-sintered $Al_2O_{3,f}$/TiAl composite decreases significantly. In the meantime, the contents of α_2 and β phases in the as-sintered composite increase with the increase of sintering temperature.

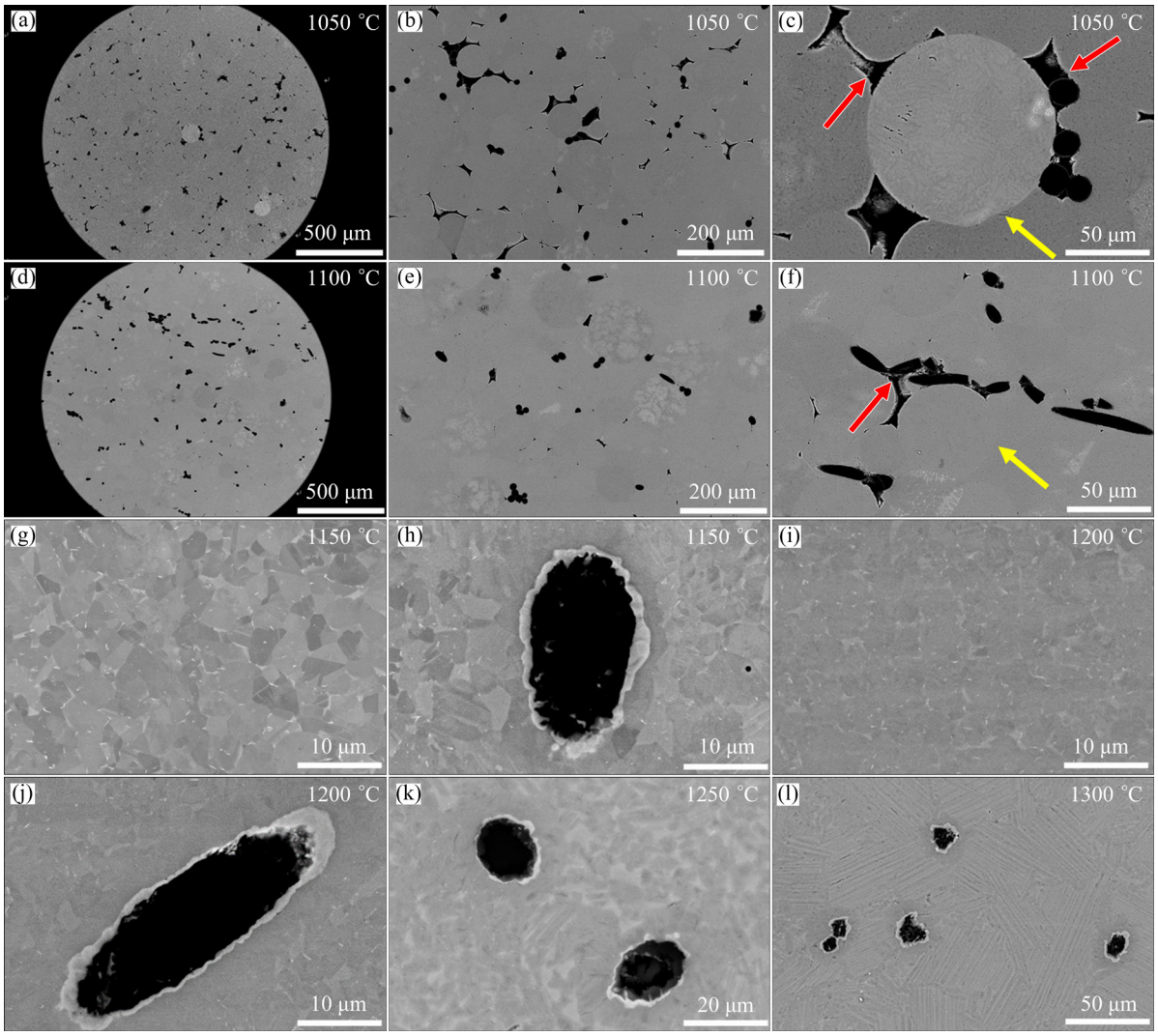

Fig. 2 Microstructures of $Al_2O_{3,f}$/TiAl composite after sintering at different temperatures: (a−c) 1050 °C; (d−f) 1100 °C; (g, h) 1150 °C; (i, j) 1200 °C; (k) 1250 °C; (l) 1300 °C

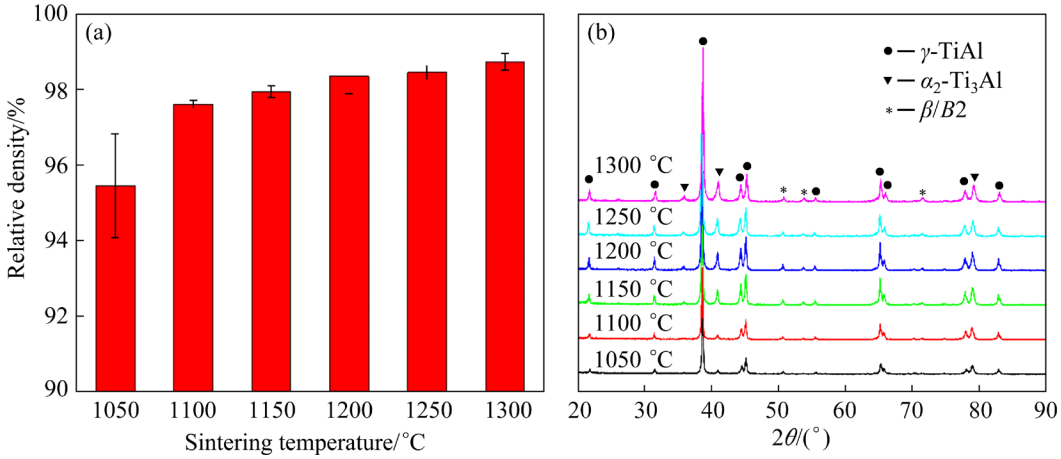

Fig. 3 Relative density (a) and XRD patterns (b) of $Al_2O_{3,f}$/TiAl composite after sintering at different temperatures

3.2 Interfacial reaction of composites

Figure 4 shows the interfacial reaction region and corresponding compositions of as-sintered $Al_2O_{3,f}$/TiAl composite at 1150 °C. The interfacial layer, as marked by arrow in Fig. 4(a), is rich in Ti and Si elements (Figs. 4(b, d)). There are relatively

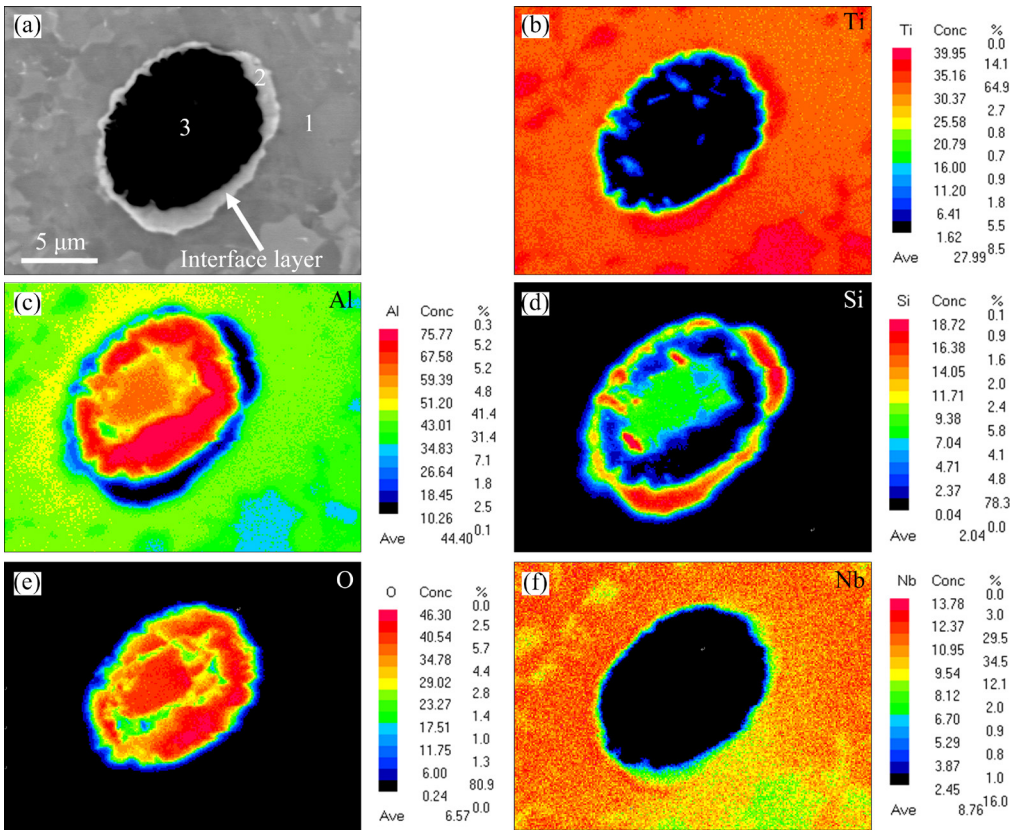

Fig. 4 Microstructures and EPMA analysis results of $Al_2O_{3,f}$/TiAl composite after sintering at 1150 °C: (a) Morphology; (b) Ti; (c) Al; (d) Si; (e) O; (f) Nb

few other elements distributed in the interfacial region (Figs. 4(c, e, f)). EPMA analysis results of matrix, interfacial layer and Al_2O_3 fiber in Fig. 4(a) are listed in Table 1. It provides further evidence of the enrichment of Ti and Si elements in the interfacial reaction region (Point 2). Compared with that of original Al_2O_3 fiber, the composition of Al_2O_3 fiber in the center of as-sintered $Al_2O_{3,f}$/TiAl composite has little change (Point 3).

Table 1 EPMA analysis results of as-sintered $Al_2O_{3,f}$/TiAl composite in Fig. 4(a) (at.%)

Point	Ti	Al	Nb	Si	O	W	B
1	44.03	45.52	6.35	0.14	3.54	0.42	–
2	46.92	10.90	5.47	19.38	11.76	0.16	5.41
3	0.17	30.69	0.01	6.17	62.96	–	–

Figure 5 shows the relationship between the thickness of interfacial reaction layer and sintering temperature in as-sintered $Al_2O_{3,f}$/TiAl composite. Among them, the interfacial reaction of the composite sintered at 1050 °C is very weak, as shown in Figs. 6(a, b). The interfacial reaction starts

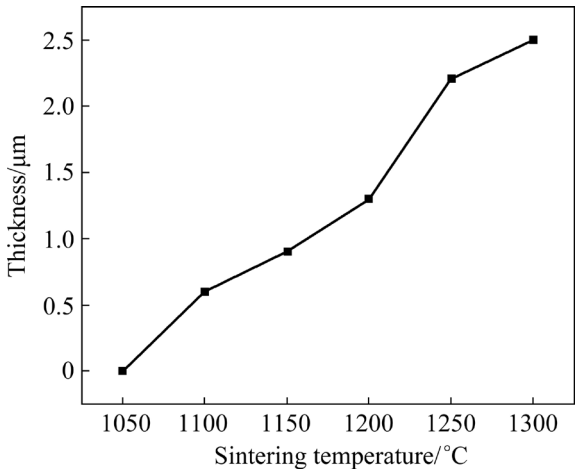

Fig. 5 Relationship between thickness of interfacial reaction layer and sintering temperature in as-sintered $Al_2O_{3,f}$/TiAl composite

to occur at 1100 °C. With the increase of sintering temperature from 1100 to 1300 °C, the thickness of interfacial reaction layer increases from 0.6 to 2.5 μm (Fig. 5). However, the interfacial reaction of the composite sintered at 1300 °C is very severe, in which the Al_2O_3 fiber tends to break down (Figs. 6(c, d)).

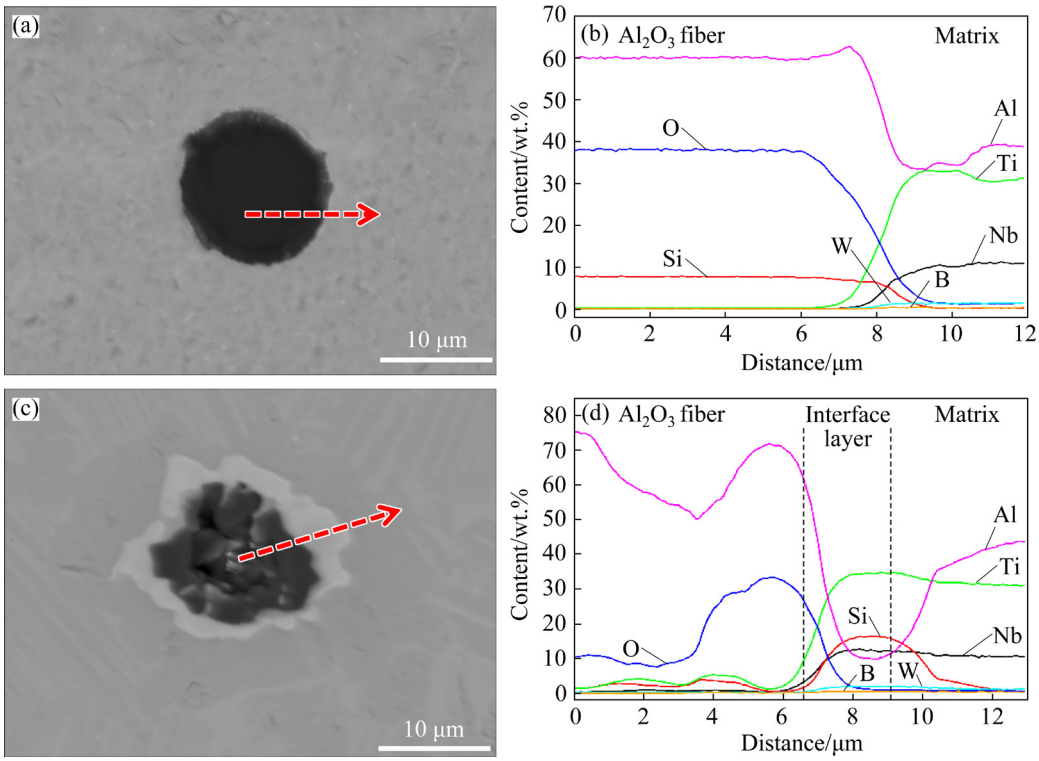

Fig. 6 Microstructures (a, c) and EPMA analyses (b, d) of $Al_2O_{3,f}$/TiAl composites after sintering at 1050 °C (a, b) and 1300 °C (c, d)

3.3 Phase evolution of composites

In order to investigate phase transformation process of Al_2O_3 fiber containing SiO_2 phase reinforced TiAl matrix composite, it is necessary to study the phase evolution of Al_2O_3 fiber. The phase changes of Al_2O_3 fiber after heat treatment at the corresponding sintering temperature are shown in Fig. 7. It can be seen that when the temperature rises to 1100 °C, the phase compositions of Al_2O_3 fiber are still γ-Al_2O_3 and amorphous SiO_2. At 1150 °C, the diffraction peaks of orthorhombic structured mullite phase appear. As the temperature increases to 1200 °C, no γ-Al_2O_3 and amorphous SiO_2 phases can be observed. In addition, a small number of θ-Al_2O_3 phase is detected. After heat treatment at higher temperatures, there is little change in the phase contents of mullite and θ-Al_2O_3 phases.

The EBSD analyses of phase evolution in $Al_2O_{3,f}$/TiAl composite sintered at 1150 °C are shown in Fig. 8. Figure 8(a) displays the micro-structure, and Fig. 8(b) shows the phase map of interfacial reaction region in the as-sintered composite. Obviously, there exists some Ti_5Si_3 phase in the interfacial layer. In addition, a small

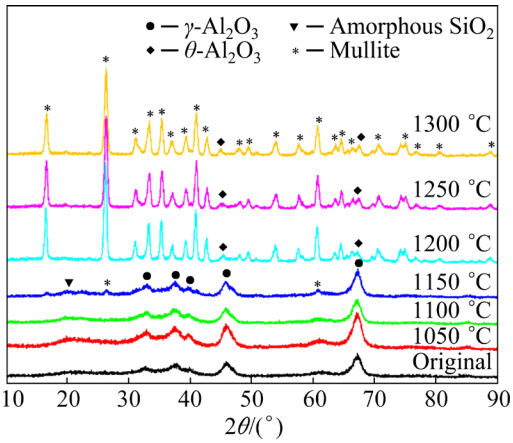

Fig. 7 XRD patterns of Al_2O_3 fiber after thermal exposure at temperatures from 1050 to 1300 °C

quantity of mullite phase is detected in the composite, as indicated by arrow in Fig. 8(b). Moreover, the remaining Al_2O_3 fiber in as-sintered composite is composed of α-Al_2O_3 phase.

3.4 Hardness

Figure 9 displays the hardness results (HV5) of $Al_2O_{3,f}$/TiAl composite at various sintering temperatures. The hardness increases rapidly with the increase of temperature from 1050 to 1100 °C,

then remains constant in the range of 1100−1200 °C, and finally decreases rapidly from 1200 to 1300 °C.

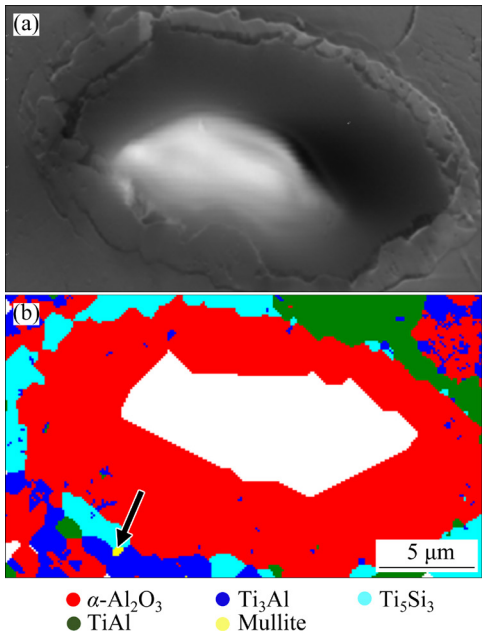

Fig. 8 Microstructures of interfacial region of $Al_2O_{3,f}$/TiAl composite after sintering at 1150 °C: (a) SEM image; (b) EBSD phase map

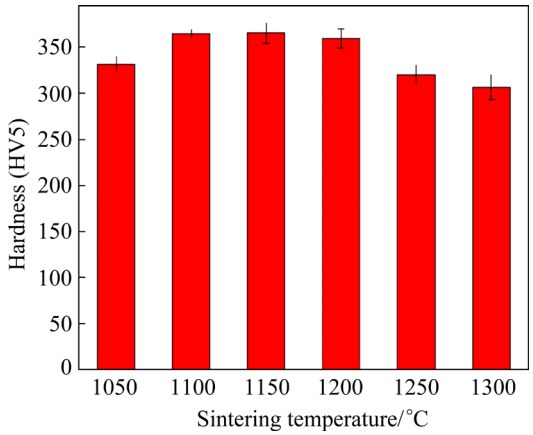

Fig. 9 Hardness of $Al_2O_{3,f}$/TiAl composite after sintering at different temperatures

4 Discussion

4.1 Thermodynamic analyses

The interfacial reaction layer was formed in Al_2O_3 fiber reinforced TiAl matrix composite, and the enrichment of Ti and Si elements in the interfacial region was identified. The interfacial reaction also affected the mechanical properties of composite, as shown in Fig. 9. The Ti atom diffused from TiAl matrix to Al_2O_3 fiber, while Si atom diffused from Al_2O_3 fiber to TiAl matrix. In fact, the affinity between Ti and Si atoms is strong [19,20]. The possible chemical reaction is shown in Eq. (1) [21,22]:

$$xTi+ySi\rightarrow Ti_xSi_y \quad (1)$$

where x and y are the stoichiometric ratios of Ti and Si, respectively. Based on the Ti−Si binary equilibrium phase diagram [23], there exist five Ti−Si compounds, i.e., Ti_3Si, Ti_5Si_3, Ti_5Si_4, TiSi and $TiSi_2$.

The Gibbs free energy change of five Ti−Si compounds in the temperature range from 1050 to 1300 °C was calculated by using Thermo-Calc thermodynamic software, and the results are shown in Fig. 10. Obviously, Gibbs free energy changes follow the sequence: $Ti_5Si_3 < Ti_5Si_4 < TiSi < Ti_3Si < TiSi_2$. Ti_5Si_3 phase exhibits the lowest Gibbs free energy change, and is thermodynamically stable. The phase analyses of as-sintered composite in Fig. 8 also prove that the interfacial reaction product is Ti_5Si_3 phase. Other studies have shown that Ti_5Si_3 phase was the major reaction product in Ti and TiAl alloys if the alloy systems contained Si elements. HUANG et al [23] investigated the interfacial microstructure of SiC reinforced Ti−6Al−4V matrix composite, and found that Ti_5Si_3 phase was mainly formed. LI and ZHANG [22] also reported the existence of Ti_5Si_3 compound in C coated SiC fiber reinforced TiAl matrix composite. The solubility of Al element in Ti_5Si_3 compound is no more than 8 at.% [24], which hinders the diffusion of Al atoms to the interfacial layer. So, Al atom is rich in the matrix, leaving behind γ-TiAl phase (Fig. 4).

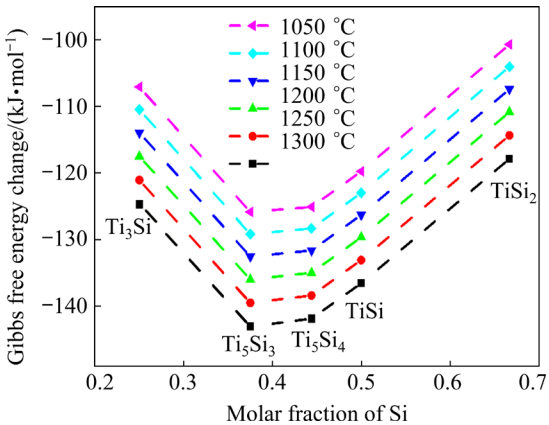

Fig. 10 Gibbs free energy changes of Ti−Si compounds in temperature range from 1050 to 1300 °C

4.2 Kinetic analyses

The interfacial reaction product Ti_5Si_3 phase is prone to the crack initiation and propagation, which is harmful to the properties of composites [13,25]. Therefore, it is necessary to analyze the growth kinetics of interfacial layer. Figure 11 exhibits the relationship between the interfacial thickness and heat treatment time at 1100 and 1150 °C. The linear relationship shows that the interfacial reaction of $Al_2O_{3,f}$/TiAl composite is mainly controlled by diffusion [26]. The growth kinetics of interfacial reaction layer can be expressed by Eq. (2) [26]:

$$z=kt^{1/2}+z_0 \tag{2}$$

where z is the interfacial thickness, k is the growth rate constant of interfacial layer, t is the thermal exposure time, and x_0 is the initial interfacial thickness before thermal exposure experiment. The growth rate constant k and temperature T satisfy the Arrhenius' relation [25]:

$$\ln k=\ln k_0-\frac{Q}{RT} \tag{3}$$

where k_0 is the pre-exponential factor, Q is the growth activation energy of interfacial layer, R is the molar gas constant and T is the thermodynamic temperature. The values of k_0 and Q are independent of temperature, depending on the chemical reaction itself.

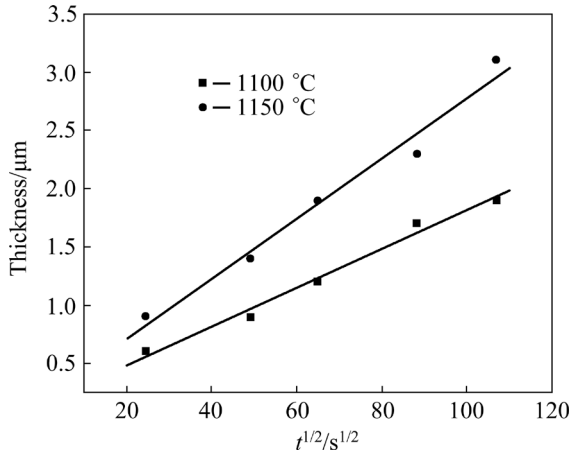

Fig. 11 Relationship between thickness of interfacial reaction layer and time in heat-treated $Al_2O_{3,f}$/TiAl composite at 1100 and 1150 °C

By fitting z–$t^{1/2}$ curves of thermal exposure experiments in Fig. 11, the growth rate constants of interfacial layer k are calculated as 1.67×10^{-8} m/s$^{1/2}$ at 1100 °C and 2.58×10^{-8} m/s$^{1/2}$ at 1150 °C, respectively. Combined with Eq. (3), the values of pre-exponential factor k_0 and activation energy Q are 4.43×10^{-3} m/s$^{1/2}$ and 285.1 kJ/mol, respectively. According to other studies [13,25], the activation energy of interfacial reaction in the SiC_f/TiAl, C-coated SiC_f/TiAl and B_4C-coated SiC_f/TiAl composites was 190, 230.7 and 308.1 kJ/mol, respectively. The activation energy of $Al_2O_{3,f}$/TiAl composite in this work is higher than that of SiC_f/TiAl and C-coated SiC_f/TiAl composites, and is close to that of B_4C-coated SiC_f/TiAl composite.

4.3 Phase changes

The Al_2O_3 fiber containing SiO_2 phase is susceptible to the occurrence of the phase transformation at high temperatures [27]. The phase compositions of Al_2O_3 fiber heat-treated at different temperatures were identified. The Al_2O_3 fiber could maintain the phase stability at 1100 °C or less. At 1150 °C, the mullite phase was formed. The formation mechanism of mullite phase was related to the chemical reaction between γ-Al_2O_3 and amorphous SiO_2 phases [28,29]. The detailed phase reaction is as follows:

$$3Al_2O_3+2SiO_2\rightarrow3Al_2O_3\cdot2SiO_2 \tag{4}$$

At the heat treatment temperature higher than 1200 °C, the crystallization process of mullite phase was completed. JIANG et al [27] also observed the mullite phase transformation in Al_2O_3 fiber.

5 Conclusions

(1) At sintering temperatures lower than 1100 °C, some pores and primary boundaries of TiAl powder particles distributed in the composite. At 1150 °C, the densification process was almost completed. With the increase of sintering temperature, the interfacial reaction became more and more severe.

(2) The interfacial phase of $Al_2O_{3,f}$/TiAl composite was Ti_5Si_3 due to the lowest Gibbs free energy change, and the interfacial reaction was controlled by diffusion of Ti atom from TiAl matrix and Si atom from Al_2O_3 fiber. The activation energy of interfacial reaction in the $Al_2O_{3,f}$/TiAl composite was 285.1 kJ/mol, which was higher than that of SiC_f/TiAl and C-coated SiC_f/TiAl composites, and was close to that of B_4C-coated SiC_f/TiAl composite.

(3) In the Al_2O_3 fiber, the mullite phase was formed after heat treatment at 1150 °C. The main phases of Al_2O_3 fiber remained to be γ-Al_2O_3 and amorphous SiO_2. The formation of mullite phase was due to the chemical reaction between γ-Al_2O_3 and SiO_2 phases. The mullite phase was also present in the composite at 1150 °C.

Acknowledgments

This work was supported by the National Science and Technology Major Project of China (No. 2019700160157).

References

[1] HU Y T, ZHENG L, YAN H J, WU L K, LIN X J, CAO F H, JIANG M Y. Improving hot corrosion resistance of aluminized TiAl alloy by anodization and pre-oxidation [J]. Transactions of Nonferrous Metals Society of China, 2021, 31: 193−206.

[2] ZHAO K, OUYANG S H, LIU Y, LIU B, LIANG X P, LI H Z, WANG Y. Isothermal oxidation behavior of TiAl intermetallics with different oxygen contents [J]. Transactions of Nonferrous Metals Society of China, 2019, 29: 526−533.

[3] ISMAEEL A, WANG C S. Effect of Nb additions on microstructure and properties of γ-TiAl based alloys fabricated by selective laser melting [J]. Transactions of Nonferrous Metals Society of China, 2019, 29: 1007−1016.

[4] REN L R, QIN S J, ZHAO S H, XIAO H Q. Fabrication and mechanical properties of Ti_2AlC/TiAl composites with co-continuous network structure [J]. Transactions of Nonferrous Metals Society of China, 2021, 31: 2005−2012.

[5] CHEN R R, ZHAO X Y, YANG Y, GUO J J, DING H S, SU Y Q, FU H Z. Effect of Zr on microstructure and mechanical properties of binary TiAl alloys [J]. Transactions of Nonferrous Metals Society of China, 2018, 28: 1724−1734.

[6] XU W C, HUANG K, WU S F, ZONG Y Y, SHAN D B. Influence of Mo content on microstructure and mechanical properties of β-containing TiAl alloy [J]. Transactions of Nonferrous Metals Society of China, 2017, 27: 820−828.

[7] LIU Z Q, MA R X, XU G J, WANG W B, SU Y H. Effects of annealing on microstructure and mechanical properties of γ-TiAl alloy fabricated via laser melting deposition [J]. Transactions of Nonferrous Metals Society of China, 2020, 30: 917−927.

[8] XU R R, LI M Q. Quantitative characterization of β-solidifying γ-TiAl alloy with duplex structure [J]. Transactions of Nonferrous Metals Society of China, 2021, 31: 1993−2004.

[9] YUAN C H, LIU B, LIU Y X, LIU Y. Processing map and hot deformation behavior of Ta-particle reinforced TiAl composite [J]. Transactions of Nonferrous Metals Society of China, 2020, 30: 657−667.

[10] CUI S, CUI C X, LV J, CHEN S Y, XIE J Q, LIU S J. Fabrication, microstructure and mechanical properties of Al_2O_3 whiskers reinforced Ti−46Al−4Nb alloy [J]. Materials Letters, 2020, 259: 126902.

[11] ZHOU M, HU R, LI J G, YANG C Y, LIU H Y, LUO X. Investigations of interfacial reaction and toughening mechanisms of Ta fiber-reinforced TiAl-matrix composites [J]. Materials characterization, 2022, 183: 111584.

[12] CUI S, CUI C X, XIE J Q, LIU S J, SHI J J. Carbon fibers coated with graphene reinforced TiAl alloy composite with high strength and toughness [J]. Scientific Reports, 2018, 8: 2364.

[13] LUO X, LI C, YANG Y Q, XU H M, LI X Y, LIU S, LI P T. Microstructure and interface thermal stability of C/Mo double-coated SiC fiber reinforced γ-TiAl matrix composites [J]. Transactions of Nonferrous Metals Society of China, 2016, 26: 1317−1325.

[14] ZHOU Y, SUN D L, WANG Q, HAN X L. Effect of fabrication parameters on the microstructure and mechanical properties of unidirectional Mo-fiber reinforced TiAl matrix composites [J]. Materials Science and Engineering A, 2013, 575: 21−29.

[15] LI J G, HU R, YANG J R, GAO Z T, ZHANG K R, WANG X Y. Evolution and micromechanical properties of interface structures in $TiNb_f$/TiAl composites prepared by powder metallurgy [J]. Journal of Materials Science, 2020, 55: 12421−12433.

[16] WEBER C H, YANG J Y, LÖFVANDER J P A, LEVI C G, EVANS A G. The creep and fracture resistance of γ-TiAl reinforced with Al_2O_3 fibers [J]. Acta Metallurgica et Materialia, 1993, 41: 2681−2690.

[17] BRUNET A, VALLE R, VASSEL A. Intermetallic TiAl-based matrix composites: Investigation of the chemical and mechanical compatibility of a protective coating adapted to an alumina fibre [J]. Acta Materialia, 2000, 48: 4763−4774.

[18] ZHOU M, HU R, LI J G, LIU H Y, LUO X. Erosion behaviors and the control of fiber structure in $Al_2O_{3,f}$/TiAl composites [J]. Journal of Alloys and Compounds, 2021, 882: 160734.

[19] YANG Y Q, ZHU Y, MA Z J, CHEN Y. Formation of interfacial reaction products in SCS-6 SiC/Ti_2AlNb composites [J]. Scripta Materialia, 2004, 51: 385−389.

[20] DAI J J, ZHANG H X, SUN C X, LI S Y, CHEN C Z, YANG Y. The effect of Nb and Si on the hot corrosion behaviors of TiAl coatings on a Ti−6Al−4V alloy [J]. Corrosion Science, 2020, 168: 108578.

[21] POLETAEV D O, AKSYONOV D A, LIPNITSKII A G. Evolutionary search for new compounds in the Ti−Si system [J]. Calphad, 2020, 71: 102201.

[22] LI X Y, ZHANG W. Interfacial reaction in SiC_f/C/TiAl matrix composites [J]. Journal of Materials Research and Technology, 2021, 12: 1227−1234.

[23] HUANG B, LI M H, CHEN Y X, LUO X, YANG Y Q. Interfacial reaction in SiC_f/Ti−6Al−4V composite by using transmission electron microscopy [J]. Materials Characterization, 2015, 109: 206−215.

[24] ZHANG K R, HU R, LEI T C, YANG J R. Refinement of massive γ phase with enhanced properties in a Ta containing γ-TiAl- based alloys [J]. Scripta Materialia, 2019, 172: 113−118.

[25] ZHANG W, YANG Y Q, ZHAO G M, FENG Z Q, HUANG B, LUO X, LI M H, CHEN Y X. Interfacial reaction studies of B_4C-coated and C-coated SiC fiber reinforced Ti−43Al−9V composites [J]. Intermetallics, 2014, 50: 14−19.
[26] YANG Y Q, DUDEK H J, KUMPFERT J. TEM investigations of the fibre/matrix interface in SCS-6 SiC/Ti−25Al−10Nb−3V−1Mo composites [J]. Composites Part A: Applied Science and Manufacturing, 1998, 29: 1235−1241.
[27] JIANG R, LIU H T, YANG L W, SUN X, CHENG H F. Mechanical properties of aluminosilicate fiber heat-treated from 800 °C to 1400 °C: Effects of phase transition, grain growth and defects [J]. Materials Characterization, 2018, 138: 120−126.
[28] LEIVO J, LINDÉN M, ROSENHOLM J M, RITOLA M, TEIXEIRA C V, LEVÄNEN E, MÄNTYLÄ T A. Evolution of aluminosilicate structure and mullite crystallization from homogeneous nanoparticulate sol−gel precursor with organic additives [J]. Journal of European Ceramic Society, 2008, 28: 1749−1762.
[29] YANG L W, WANG J Y, LIU H T, JIANG R, CHENG H F. Sol−gel temperature dependent ductile-to-brittle transition of aluminosilicate fiber reinforced silica matrix composite [J]. Composites Part B: Engineering, 2017, 119: 79−89.

Al_2O_3 纤维增强 TiAl 基复合材料的界面反应

罗耀峰，陆锐宇，王 岩，刘 彬，阳海棠，刘 咏

中南大学 粉末冶金国家重点实验室，长沙 410083

摘 要：采用电火花等离子烧结(SPS)制备 Al_2O_3 短纤维(含 28%(体积分数)SiO_2) 增强 TiAl 基复合材料。通过热力学和动力学分析，阐明界面反应机理。基体与 Al_2O_3 纤维的界面相为 Ti_5Si_3，该相主要来源于 TiAl 基体中的 Ti 元素和 Al_2O_3 纤维中的 Si 元素。TiAl 基体与 Al_2O_3 纤维的界面反应激活能为 285.1 kJ/mol。此外，由于界面反应过程中 Ti 元素的消耗，界面周围的基体由 γ-TiAl 相组成。在热处理态 Al_2O_3 纤维和烧结态复合材料中，γ-Al_2O_3 与非晶态 SiO_2 相发生化学反应，形成莫来石相。

关键词：TiAl 基复合材料；界面反应机理；Al_2O_3 纤维；相变；致密化机理

(Edited by Bing YANG)